HHS Public Access

Author manuscript

Cell Physiol Biochem. Author manuscript; available in PMC 2020 March 30.

Published in final edited form as:

Cell Physiol Biochem. 2019 ; 52(5): 1017–1038. doi:10.33594/000000070.

Expression, Localization and Functional Activity of the Major Na^+/H^+ Exchange Isoforms Expressed in the Intestinal Cell Line Caco-2BBe

Yan Yu[a], **Anna Seidler**[a], **Kunyan Zhou**[a], **Zhenglin Yuan**[a], **Sunil Yeruva**[a], **Mahdi Amiri**[a], **Chris C. Yun**[b], **Katerina Nikolovska**[a], **Ursula Seidler**[a]

[a]Department of Gastroenterology, Hannover Medical School, Hannover, Germany

[b]Division of Digestive Diseases, Department of Medicine, Emory University, Atlanta, GA, USA

Abstract

Background/Aims—Enterocytes express a number of NHE isoforms with presumed localization in the apical (NHE2, 3 and 8) or basolateral (NHE1) membrane. Functional activity and localization of enterocyte NHE isoforms were assessed using fully differentiated Caco-2BBe cells, whose genetic expression profile closely resembles mature enterocytes.

Methods—The activity of the different NHEs was analyzed by fluorometric pH_i-metry in a perfusion chamber with separate apical and basolateral perfusion, using specific inhibitors and shRNA knockdown of NHE2. The expression of the NHEs and of other relevant acid extrusion transporters was quantified by qPCR.

Results—Quantitative comparison of the mRNA expression levels of the different NHE isoforms in 14 day-differentiated Caco-2BBe cells showed the following order: NHE2>NHE8>NHE3>NHE1. Acid-activated NHE exchange rates in the basolateral membrane were >6-fold higher than in the apical membrane. 79 ± 3 % of the acid-activated basolateral Na^+/H^+ exchange rate displayed a NHE1-typical inhibitor profile, and no NHE2/3/8 typical activity could be observed. Analysis of the apical Na^+/H^+ exchange rates revealed that approximately 51 ± 3 % of the total apical activity displayed a NHE2/8-typical inhibitor profile and 31 ± 6 % a NHE3-typical inhibitor profile. Because no selective NHE2 inhibitor is available, a stable NHE2 knockdown cell line (C2NHE2KD) was generated. C2NHE2KD displayed a reduced NHE2-typical apical Na^+/H^+ exchange rate and maintained a lower steady-state pH_i, despite high expression levels of other acid extruders, in particular NBCn1 (Slc4a7).

Conclusion—Differentiated Caco-2BBe cells display particularly high mRNA expression levels of NHE2, which can be functionally identified in the apical membrane. Although at low

Prof. Dr. Ursula Seidler and Dr. Katerina Nikolovska, Department of Gastroenterology, Hepatology and Endocrinology, Hannover Medical School Carl Neuberg Straße 1, D 30625 (Germany); Tel. +49 511 532 9427, Fax +49 511 532 8428, Seidler.Ursula@mh-hannover.de; Nikolovska.Katerina@mh-hannover.de.
K. Nikolovska and U. Seidler contributed equally to this work.

Disclosure Statement

The authors have no ethical conflicts to disclose. The authors have no conflicts of interest to declare.

intracellular pH, NHE2 transport rate was far lower than that of NHE1. NHE2 activity was nevertheless essential for the maintenance of the steady-state pH_i of these cells.

Keywords

pHi-regulation; Enterocyte; Intestinal electrolyte transport; NHE2; NHE3; NHE8; NBCn1

Introduction

Different Na^+/H^+ exchanger isoforms of the SLC9 gene family are expressed in the basolateral and apical membranes of epithelial cells as well as on the intracellular organelles [1–3]. While the cellular expression, localization and physiological functions of NHE1 (SLC9A1) and NHE3 (SLC9A3) have been extensively characterized, the role of the other isoforms is far less understood. NHE2 (SLC9A2) is highly expressed in the gastrointestinal tract, presumably in an apical location [4, 5], but basal/intracellular staining has also been reported [6]. Nevertheless, NHE2 knockout (*slc9a2*$^{-/-}$) mice do not develop an increase in stool water, and the additional deletion of NHE2 does not result in a more severe phenotype than that of NHE3 alone [7]. In contrast to NHE3 knockout (*slc9a3*$^{-/-}$) mice, *slc9a2*$^{-/-}$ mice did not display differences in jejunal fluid absorptive rates compared to wild type (*wt*) littermates [8]. NHE2 is activated by short chain fatty acids (SCFA) [9] and has been implicated in butyrate-stimulated fluid absorption in colitic rats [10]. However, the role of the NHE isoforms in SCFA-stimulated fluid absorption is controversial [11–14] and is even more complicated by the recent delineation of multiple SCFA-dependent Na^+ transporting mechanisms [15]. Thus, the functional significance of intestinal NHE2 requires further study.

The elucidation of the molecular properties of NHE2 is equally incomplete. Heterologous expression of NHE1–3 in AP1 cells (NHE-deficient CHO cells) and in PS120 cells (NHE-deficient fibroblasts) yielded comparable basic characteristics for NHE1 and for NHE3 in the two cell lines, but the NHE2 characteristics differed in their response to hyperosmolarity [16, 17]. Heterologous overexpression of NHE2 in renal medullary collecting duct (mIMCD-3) cells has resulted in a downregulation of NHE3 expression and apparent basolateral appearance of hyperosmolarity-activated NHE2 activity [18]. NHE2 was also expressed in intestinal cell lines, and it was suggested that the cell type was important to reproduce (not yet well understood) physiological NHE2 characteristics [19]. The study of endogenous NHE2 is hampered by the scarcity of NHE2-expressing cell lines, lack of commercially available antibodies, ambiguity about NHE2 membrane expression, and an overlapping inhibitor profile with other NHE isoforms.

Heterologous NHE2 traffics either to the apical membrane [17, 20] or the basolateral membrane in renal mIMCD-3 collecting duct cells [18]. The apical targeting of NHE2 depends on the presence of a SRC homology domain (a domain also found in the tyrosine kinase SRC oncoprotein) that binds to a number of proteins, which may be involved in the determination of membrane localization [17]. This raises the possibility that NHE2 trafficking is regulated and cell-type dependent. When expressed in PS120 fibroblasts or

Caco2 cells, the half-life of NHE2 is markedly shorter than that of NHE1 and NHE3 [21]. This observation has not been followed up for endogenously expressed NHE2.

In the intestine, the only antibody whose specificity was tested in knockout tissue localized NHE2 to the upper part of the gastric glands and the lower part of the colonic crypts, both areas of epithelia in which Na^+ absorption is not a prominent feature in intestinal transport physiology, or has not been assessed [9]. Endogenous Na^+/H^+ exchange with an "NHE2-typical inhibitor profile", after treatment with different inhibitors, has been observed in intestinal cell lines [9, 22] as well as in murine colonic crypts [5, 23]. Since the inhibitors both display a significant overlap for the other expressed NHE isoforms, or were not applied separately to the apical vs basolateral enterocyte membrane, the relative contribution of NHE2 to the observed overall Na^+/H^+ exchange rate remained nevertheless uncertain.

Recently, inhibitors have been developed that potentially permit a better separation of the transport activity of NHE1, 2 and 3 than the classic NHE inhibitors amiloride and derivatives, HOE694, S3226 and S1611 [24–26]. We therefore screened available gastrointestinal cell lines for NHE expression. The self-differentiating clonal Caco-2BBe cells were chosen due to their high expression of NHE2, a method was developed to separately study apical and basolateral NHE activity, and the inhibitor concentrations to selectively inhibit NHE isoforms in the apical and basolateral membrane were established. NHE2 was silenced by shRNA and apical and basolateral NHE activity was assessed in fully differentiated NHE2-silenced (C2NHE2KD) and mock-silenced Caco-2BBe (C2PLKO.1) with and without application of the tested inhibitor concentrations.

Materials and Methods

RNA isolation and qPCR

The Caco-2BBe, C2PLKO.1 and C2NHE2KD cells were seeded at the density of $1.5 \times 10^4/cm^2$ and $3 \times 10^4/cm^2$, respectively, and cultured on transwell membranes (pore size 0.4 μm) for 14 days. On the 14th day, cells were harvested for RT-PCR analysis. Cell lysate was homogenized with QIAshredder homogenizer and the total RNA was extracted from the cells using the RNeasy® Mini Kit (Qiagen GmbH) following the guidance of the instruction manual. RNA quality was determined by capillary gel electrophoresis with the QIAxcel® system (Qiagen GmbH). 1 μg RNA was reverse transcribed with the QuantiTect® Reverse Transcription Kit (Qiagen GmbH) and cDNA concentration was measured spectrophotometrically. cDNA was diluted 1:20 with DNase free water and 2 μL of the dilution was used as a template for PCR. Each reaction additionally contained 5 μL 2× MESA Green qPCRMasterMix (Eurogentec GmbH) and an appropriate amount of primers (Supplementary Table 1 - for all supplemental Material see www.cellphysiolbiochem.com).

Lentiviral mediated NHE2 knockdown in Caco-2BBe Cells

Bacterial glycerol stocks containing PLKO.1 lentiviral vector harboring five individual, small hairpin RNA (shRNA) constructs against human NHE2 (SHCLNG-NM-003048) were obtained from Sigma (St. Louis, USA) and were used to generate lentiviral particles as described earlier [27]. To evaluate the knockdown efficiency of individual shRNA against

NHE2 lentiviral transduction was done as follows: Caco-2BBe cells (source ATCC® CRL-2102, kindly provided by Georg Lamprecht, Rostock) were plated at a density of 5×10^4 cells per well in 24 well plates and incubated at 37°C and 5% CO_2 until they reached 60–70% confluence. Then the medium from the wells was removed and replaced with medium containing 5 μg/mL Polybrene. Equal volumes of lentivirus were added to the medium and cells were incubated overnight in Polybrene containing medium. Then the medium was replaced with normal medium and incubated for another 24 hours before cells were harvested and NHE2 expression was analyzed by real time PCRs (in absence of an antibody to detect human NHE2 by Western blot). shRNA 1, 4 and 5 showed approximately 50 % knockdown of NHE2 mRNA. In order, to achieve higher knockdown of NHE2, Caco-2BBe cells were transduced with these three shRNAs together, selected with 15 μg/mL puromycin, and maintained with 10 μg/mL puromycin. Real-time PCRs performed after stable selection of the cells showed > 80 % knockdown of NHE2 mRNA (Supplementary Fig. 1).

Cell proliferation assay

C2NHE2KD and C2PLKO.1 cells were cultured as described above and left to reach subculturing density of 70% confluence. Cells were detached with 0.5 % trypsin / 0.53 mM EDTA in PBS for 5 min at 37°C and 5% CO_2. Trypsin action was arrested by addition of 2 mL of complete medium and cell suspension was centrifuged 5 min at 1500 rpm. After removing supernatant, cell pellet was resuspended in complete medium and seeded at 0.13 $\times 10^4/cm^2$ in 24 well plates. The cells were counted daily for a period of 16 days, using Hemocytometer. During the time of the assay the medium was changed every 48 hours.

Cell adhesion assay

C2PLKO.1 and C2NHE2KD cells were seeded onto 96 well plate at a density of 1×10^4 cells /well and cultured for 24 hours. Cells were washed vigorously to remove non-adhered cells prior to acquiring pictures with phase contrast microscope. Cells were counted at 5 different regions for each well. The average value for each well was used to calculate the mean value for cell adhesion.

Overexpression of human NHE3 in Caco-2BBe cells (source C. Yun, Emory University)

Caco-2BBe cells were transfected with full length human NHE3 tagged with VSVG (with the amino acid sequence YTDIEMNRLGK derived from the Vesicular Stomatitis viral glycoprotein) at C-terminus (a kind gift from Chris Yun, Emory University, Atlanta, USA with the permission of use from Ming Tse, John Hopkins University, Baltimore) and stable cell lines were established using 800 μg/mL G418 (Promo cell GmbH, Heidelberg, Germany) in the medium. The cells were grown at 37°C in a humidified atmosphere containing 5% CO_2, in Dulbecco's Modified Eagle Medium with 4.5 g/l D-glucose and sodium pyruvate (Life Technologies GmbH, Darmstadt, Germany) supplemented with 10% fetal calf serum (FCS), 100 units/mL penicillin, 100 μg/mL streptomycin and 1% non-essential amino acids. The cells were maintained with 800 μg/mL G418 antibiotic in the medium. Then the cells were subjected to repeated acid selection for 5 cycles as described previously [28]. After 5 acid suicide selection cycles, the expression of NHE3-VSVG

protein expression using anti-VSVG antibody and a robust NHE3 protein expression was detected (Supplementary Fig. 2).

Immunofluorescence staining of Caco-2BBe cells

C2PLKO.1 and C2NHE2KD cells were seeded at the density of $1.5\times10^4/cm^2$ and $3\times10^4/cm^2$, respectively, on 0.4 μm transwell filters and incubated for 14 days. The cells were fixed in 4% paraformaldehyde solution for 20 min and washed with PBS. Cells were incubated with CFTM633 Wheat Germ Agglutinin (WGA) staining solution (5 μg/mL in HBSS without phenol red) for 10 minutes at 37°C according to manufacturer instruction (Biotium, Inc. USA). After washing with PBS, cells were permeabilized for 5 min with 0.2 % triton X-100 solution. 5 % goat serum/PBS for 30 min was used to block unspecific binding. The cells were incubated with occludin (mouse monoclonal anti-occludin antibody (clone OC-3F10) 2 μg/mL in PBS for 3 h. Goat anti-mouse Alexa 555 conjugated IgG (H+L) 1 μg/mL was used as a secondary antibody and 1 μg/mL Hoechst 33258 to label the nuclei. Membranes were mounted on cover glasses and sealed with coverslips. Samples were analyzed using 40× and 63× objectives on Leica DM IRB with a TCS SP2 AOBS scan head confocal microscope. Images were obtained in both xyz and xzy modes.

Fluorometric determination of apical and basolateral acid-activated NHE (and other potential acid/base transporter) activity

C2PLKO.1 (mock-silenced), C2NHE2KD (NHE2-silenced) or C2NHE3vsv (acid-suicide-selected NHE3 overexpressing) cells were seeded onto transwell membranes (pore size 3 μm) at the density of $1.5 \times 10^4/cm^2$ or $3 \times 10^4/cm^2$ (for C2NHE2KD), and cultured for 14 days to allow formation of well-differentiated monolayer. Cells between passage 12 and 15 were used for these experiments. For each cell line, 5 experiments involving 4–5 different passages were done for each perfusion method unless otherwise indicated. The transwell membranes were cut off from the inserts and placed into the perfusion chamber with the apical side towards to fluorescent light path and the basal side facing the investigator (Supplementary Fig. 3). The chamber was fixed on the stage of an inverted microscope (Zeiss, Germany). Cells were loaded with 5 μM BCECF-AM (Life Technologies GmbH, Darmstadt, Germany) exclusively from the basolateral side for 30 min at 37°C. A long distance 20x objective was used to focus on the cells through the apical perfusion chamber. The dimensions of the perfusion chambers were 7 mm x 2 mm x 2mm.Cell fluorescence was alternately excited at 440 nm and 495 nm at a rate of 100/s and emitted at 520 nm. Data acquisition and processing were performed using the Metafluor software. Emitted light was collected through a 510 nm dicroic mirror, a 530 nm long-pass filter, and an adjustable diaphragm and recorded by a photomultiplier. Background fluorescence intensity was measured and subtracted during calculation.

Na^+ dependent pH_i recovery after NH_3/NH_4^+ prepulse-induced intracellular acidification in the absence of CO_2/HCO_3^- was used to investigate NHE activity (Na^+/H^+ exchange activity) [29, 30]. Independent measurement of NHE activity on either apical or basolateral side of differentiated Caco-2BBe cell monolayer was accomplished by adding Na^+ only to the solution perfusing the apical or that perfusing the basolateral membrane, respectively. The buffer compositions of buffer A-E are given in Supplementary Table 2. Buffers A to E were

prepared on the day of the experiment or in the evening before and were titrated to assigned pH at 37°C, and equilibrated with synthetic air (18% O_2, 82% N_2, Linde Gas, Hannover). The flow rate was 2 mL per minute, resulting in a very fast fluid exchange in the tiny chamber volume. The chamber perfusate was maintained at 37°C by setting the temperature to 42°C in the buffer reservoir and taking the cooling during gravity-drainage perfusate flow into account. A calibration curve (fluorescence vs. pH) is generated by incubating cells in a high potassium buffer at various pH values in the presence of the K^+/H^+ ionophore, nigericin. NHE inhibitors were kind gifts of Sanofi-Aventis (Frankfurt, Germany), from AstraZeneca (Malmö, Sweden) or purchased from Adooq chemicals (Irvine, CA) or from Merck, Germany.

The steepest ΔpH_i/second slope was defined as the highest pH_i recovery rate (dpH/dt), and dpH/dt was averaged over 60 seconds within that time frame of steepest initial pH_i rise after Na^+ addition. Care was taken to exactly determine the time lines necessary to achieve closely similar pH_i values before the re-addition of Na^+, and these pH_i values are given in the figures.

To search for potential acid extrusion mechanism for the alternative transporters that are responsible for residual Na^+-dependent pH_i-recovery that is insensitive to 60 μM HOE642 and tenapanor, the same experimental protocol was performed in the presence of the specific MCT-1 inhibitor AZD3965 (MedChemExpress, Sollentuna, Sweden) (500 nM overnight, and 1 hour preincubation, and 500 nM presence in the apical perfusate) and the anion transport inhibitor DIDS (1mM to inhibit NBCe1/e2 in the basolateral perfusate).

Steady-state pH_i measurement Caco-2BBe cells

To analyze the steady state pH_i of the C2PLKO.1 and C2NHE2KD cells in presence of CO_2/HCO_3^- the same experimental setup described above was used. The cells were perfused with buffer A solution (100 mM NaCl, 24 mM $NaHCO_3$, 10 mM D-glucose, 0.5 mM K_2HPO_4, 5 mM KCl, 1 mM $MgCl_2 \times 6H_2O$, 2 mM $CaCl_2$x-$2H_2O$, 11 mM HEPES, pH7.4) for at least 20 minutes at 37°C gassed with O_2/CO_2 before fluorescence ratio recording. Then the emission signal was recorded for an additional 20 minutes, before the cells were perfused with two different pH calibration solution (10 mM D-glucose, 0.5 mM K_2HPO_4, 135 mM KCl, 1 mM $MgCl_2$, 2 mM $CaCl_2$, 11 mM HEPES pH 7.0 or pH 7.4) with 10 μM nigericin. Finally the ratio of 495/440 was converted into respective pH value by linear curve fitting.

Statistics

The data were analyzed with GraphPad Prism 6. Results were expressed as means ± SEM. Experiments were performed 5 times, if not otherwise indicated. All techniques mentioned above were carried out using 4 different passages of each cell line. Data were compared by unpaired two-tailed Student's t-test (two groups) or one-way ANOVA (more than two groups) with subsequent Tukey's multiple comparison tests. $P < 0.05$ was considered to be significant, * $p < 0.05$, ** $p < 0.001$, *** $p < 0.0001$.

Results

NHE1–3 and 8 mRNA expression levels in 14 day differentiated Caco-2BBe cells

Caco-2BBe cells were harvested after 14 days culture, as described in material and methods, mRNA was extracted and the mRNA expression of the NHE1–3 and NHE8 were assessed using β-actin and villin as control genes. Fig. 1A demonstrates the mRNA expression levels of the four NHE isoforms with β-actin as control gene, while in Fig. 1B the brush border marker villin was used as control gene. NHE2 had the highest mRNA expression levels in relation to either control gene, followed by NHE8>NHE3>NHE1.

Characterization of the NHE2-silenced (C2NHE2KD) cell line in comparison to a mock-silenced cell line (C2PLKO.1)

After testing a variety of NHE2-silencing protocols, we established two additional Caco-2BBe cell lines, one in which NHE2 expression was downregulated by shRNA-mediated gene silencing named C2NHE2KD, and the other one was treated with the scrambled shRNA (mock-silencing) and named C2PLKO.1. NHE2 downregulation was ~ 80 % in the C2NHE2KD cell line in subconfluent cell cultures from the initial cell passages (Supplementary Fig. 1). The basic characteristics of these two cell lines were compared with each other and the mother cell line. The C2NHE2KD cells had reduced plating efficiency compared to C2PLKO.1 cells (Fig. 2A, B). For this reason the number of C2NHE2KD cells seeded was doubled compared to C2PLKO.1 cells (3.0 vs. 1.5×10^4 cells/cm^2) and all subsequently described experiments are performed in this fashion. The proliferation rate was delayed in C2NHE2KD compared to C2PLKO.1 cells in the subconfluent stage, while after confluency, the cell replication rates slowed and became equal between the two cell lines (Fig. 2C). Transepithelial resistance (TEER) was measured daily and was lower in C2NHE2KD compared to C2PLKO.1 in the initial postconfluent state and then increased to levels above that of C2PLKO.1 (Fig. 2D). Immunofluorescent analysis of the monolayers (using occludin) in xyz and xzy scanning mode, revealed that at 14 days of culture, the C2NHE2KD were flatter compared to the C2PLKO.1 cells (Fig. 2E).

Determination of NHE3 inhibition by tenapanor

Next, suitable NHE inhibitor concentrations for a clear separation of NHE1, NHE2/8 and NHE3 were determined. Previous experiments in our lab with NHE1-transfected PS120 cells and NHE1 expressing RGM-1 cells had suggested that at physiological Na^+ concentrations, 3 μM HOE642 is required to fully inhibit NHE1, a concentration which will already inhibit transfected NHE2 by ~ 20% [31]. 50–60 μM HOE642 fully inhibits NHE2 with no obvious inhibition of NHE3 [32]. Since the NHE3 inhibitor S1611 inhibits rodent and possibly human NHE1 in the high concentrations required to fully inhibit NHE3, the new NHE3-selective drug tenapanor was tested. To do so, Caco-2BBe cells, which do not express high endogenous levels of NHE3 [22], were transfected with human Vesicular Stomatitis Virus Glycoprotein (VSV-G) epitope-tagged NHE3, and acid-suicide selected Caco-2BBe/hNHE3vsv cells were grown on 3 μm pore size filters. TEER of these cells was measured daily (Fig. 3A). Fig. 3B–D shows the pH_i-traces of the different experimental protocols. Basolateral NHE activity was inhibited by complete Na^+ removal from the basal perfusate. The rapid flow rate of 2 mL/min and the small volume of the basal chamber (a few μl)

ensured that Na^+ permeation from the apical side, should it occur, would not influence the results. This concept was validated by adding 3 μM HOE642 to the basal perfusate, which did not influence the results. While apical 60 μM HOE642 did not significantly influence apical NHE activity, the co-perfusion with 1 μM tenapanor completely inhibited NHE3 activity (Fig. 3E). The same concentration of tenapanor did not affect basolateral NHE activity (data not shown). This suggests that 1 μM tenapanor in the apical bath is able to fully inhibit human NHE3 activity.

Comparison of NHE1, 3 and 8 mRNA expression levels in C2NHE2KD and C2PLKO.1

The two cell lines were plated with 1.5 and 3.0×10^4 cells/cm^2 on transwell filters, and grown for 14 days. RNA extraction and qPCR were performed as described in material and methods. The results are shown in Fig. 4A–D. A significant upregulation of NHE8 mRNA expression was observed in C2NHE2KD compared to C2PLKO.1 cells. Because no alteration in mRNA expression levels for the NHEs was detected between the Caco-2BBe and the C2PLKO.1 cell line (for comparison Fig. 1A and Fig. 4), subsequent experiments were performed with the C2PLKO.1 and the C2NHE2KD cell lines.

Basolateral Na^+/H^+ exchange rates in C2PLKO.1 cells and effect of NHE inhibitors

In order to functionally localize NHE2 activity and therefore its expression, the total NHE activity and the proportion inhibited by 3 μM or by 60 μM HOE642 was fluorometrically assessed in the basolateral membrane of C2PLKO.1 cells. Fig. 5A–C show the separate pH_i-traces of the different inhibitors applied. The ΔpH_i/min in the initial fast phase of pH_i recovery with/without inhibitor is shown in Fig. 5D. The pH_i values after NH_4^+-induced acidification, before the re-addition of Na^+ (plus inhibitors) to the basolateral perfusate were comparable between the different experimental conditions as shown in Fig. 5E. Basolateral Na^+-dependent pH_i recovery rate was 0.31±0.026 in the absence of inhibitors (5D, first column). In the presence of 3 μM HOE642 this basal activity was inhibited by 79±2.8% and the percentage of inhibition was not changed when the inhibitory concentration of HOE642 was increased to 60 μM (80.7±2.3%). The result suggested that the predominant basolateral NHE is NHE1. Furthermore, no evidence for NHE2 activity was observed in the basolateral membrane.

Effect of NHE isoform specific inhibitors on apical Na^+/H^+ exchange activity in C2PLKO.1 cells

To address the putative apical activity of NHE2, NHE8 and NHE3, the Na^+-free basolateral perfusate was maintained after the NH_4^+-repulse to block all basolateral NHE activity, and Na^+ was added selectively to the apical bath with and w/o inhibitors (Fig. 6A–F). Total apical Na^+/H^+ exchange activity was approximately 6 fold lower than basolateral Na^+/H^+ rates (compared the first scatterplot of Fig. 5D with that in Fig. 6E), which was surprising given the fact that NHE1 mRNA expression was far lower than that of all NHE isoforms named above. 60 μM HOE642 will fully inhibit NHE2 (and likely NHE8, which has been shown to be sensitive to 10 μM HOE694), but will leave NHE3 active, and resulted in a 51±3.1% inhibition of total apical NHE activity (Fig. 6B, E). 1 μM tenapanor resulted in a 30.8±5.6% inhibition (Fig. 6C, E), and the combination of the two inhibitors resulted in an 82.3±3.1% inhibition (Fig. 6D, E). The remaining Na^+-dependent proton efflux or base

influx may be mediated by base or proton channels, or an NBC accepting OH^- for transport. Although this approach cannot distinguish between NHE2 and NHE8 activity, it nevertheless demonstrates that the two NHE isoforms with the highest mRNA expression result in very little acid-activated NHE activity in the apical membrane of Caco-2BBe cells.

Total Na+/H+ exchange activity in C2PLKO.1 and C2NHE2KD cells

In order to investigate the effect of the loss of NHE2, the total Na^+/H^+ exchange activity during pH_i-recovery from an a NH_4^+prepulse-induced intracellular acid load was compared between the C2NHE2KD and C2PLKO.1 cells. The total NHE activity was assessed using the same technique described above by perfusing both apical and basal sides of the cell monolayer with Na^+-solution in the absence of inhibitors during the pH_i recovery period. Representative curves are shown in Fig. 7A, B. Despite the reduced expression of NHE2 in the C2NHE2KD no difference in the total Na^+/H^+ exchange activity was detected compared to C2PLKO.1 cells (Fig. 7C). The initial pH_i at the beginning of the pH_i recovery is shown in Fig. 7D.

Basolateral Na^+/H^+ exchange activity in C2NHE2KD cells

The same experiments as described in Fig. 5 were repeated with the NHE2-silenced cells C2NHE2KD. As evidenced in Fig. 8A–E, the total NHE activity and relative inhibitor sensitivities of acid-induced basolateral Na^+/H^+ exchange did not differ significantly in the C2NHE2KD compared to C2PLKO.1 cells, confirming that NHE1 is the main NHE on the basal side of both C2NHE2KD and C2PLKO.1 cells.

Apical Na^+/H^+ exchange activity in C2NHE2KD cells

Total apical NHE activity was not significantly different in C2NHE2KD compared to C2PLKO.1 cells (0.050±0.005 vs 0.046±0.003 ΔpH_i/min), but the percentage inhibited by the different pharmacological agents was altered (Fig. 9A–F). The percentage of acid-activated NHE activity that was inhibited by 60 μM HOE642 (NHE2 inhibition) was reduced to 40.6±3.8%, that inhibited by 1 μM tenapanor (NHE3 inhibition) was virtually unaltered, and that not inhibited by 60 μM HOE642 and 1 μM tenapanor was increased to 28.1±2.1%.

Acid extrusion mechanisms that may explain the non-NHE inhibitor sensitive Na^+-dependent basolateral pH_i recovery

Inhibition of NHE1 at the basolateral membrane uncovered existence of Na^+-transporters that are not sensitive to high concentrations of HOE642. One obvious candidate is NHE4. Although rat intestinal NHE4 expression is reportedly low to nonexistent [33, 34], and NHE4-deficient mice displayed no intestinal phenotype [35, 36], its insensitivity to specific NHE inhibitors (except high concentrations of dimethyl-amiloride which inhibits a number of non-NHE transporters in these high concentration) makes it difficult to study its function. However, expression and functional activity has been reported in human enterocytes by some [37, 38], while reported absent by others [39, 40]. For the low residual Na^+-dependent pH_i-recovery, we therefore believe that it is one candidate that cannot easily be ruled out experimentally.

Amiloride-insensitive Na^+ absorption may be also related to the function of Na^+/HCO_3^- cotransporters (NBC). mRNA expression analysis revealed high expression of electroneutral Na^+-HCO_3^- cotransporter NBCn1 (SLC4A7), compared to the electrogenic Na^+/HCO_3^- cotransporter NBCe1 (SLC4A4) and the Na^+-dependent Cl^-/HCO_3^- exchanger NBCn2 (SLC4A10) (Fig. 10A), however without significant differences between the C2NHE2KD and the C2PLKO.1 cells. The majority of the SLC4A HCO_3^- transporters except NBCn1 are sensitive to stilbene derivatives such as DIDS [41, 42]. However, presence of 1 mM DIDS in the basolateral perfusion bath of both C2NHE2KD and the C2PLKO.1 cells did not affect the Na^+-dependent pH_i recovery rate compared to non-treated cells in the absence of CO_2/HCO_3^-(Fig. 10B, D, F). Furthermore co-perfusion with 3 μM HOE642 and 1 mM DIDS showed no differences in pH_i recovery rate compared to treatment with only 3 μM HOE642 (Fig. 10C, E, F). Therefore, we believe that based on the high expression levels, the DIDS-insensitive NBCn1 is likely an important pH_i regulator in HCO_3^- containing medium, and, based on the ability of the cells to endogenously produce CO_2 and convert it to HCO_3^- with the help of their intra- and extracellular carbonic anhydrases, may also mediate a part of the HOE642-insensitive residual base influx observed in our experiments.

Experiments performed to address the potential residual apical proton extrusion mechanism were also performed (suppl. Fig. 4), however, could not identify involved transporters.

Steady-state pH_i in C2PLKO.1 and C2NHE2KD cells in the absence and presence of CO_2/ $HCO3^-$

In order to assess the steady-state pH_i, cells were incubated in either HEPES-containing medium in an incubator with air, or a HCO_3^- containing medium in a CO_2-gassed incubator. The pH of the medium was 7.4 in both instances. Transwell membranes with cells were then mounted on the perfusion chamber, loaded with BCECF and perfused bilaterally in presence or absence of CO_2. After 30 min of stable readings, pH_i calibration was performed with pH values that are closely above and below the expected pH_i. The results in Fig. 11 demonstrate that both in HEPES and in HCO_3^- containing medium, the pH_i of the C2NHE2KD cells was lower than the C2PLKO.1 cells (Fig. 11A, B).

Discussion

The current study investigates the molecular nature of apical and basolateral NHE activity in the self-differentiating gastrointestinal cell line Caco-2BBe and compares the mRNA expression levels for the different NHE isoforms 1, 2,3 and 8 with the isoform-specific functional activities attributed by inhibitor experiments. A combination of selective Na^+ addition to the apical or basolateral membrane, a set of NHE-isoform specific inhibitor concentrations, as well as shRNA-mediated silencing of NHE2 were utilized to assess the involvement of the different NHEs in pH_i-recovery from a NH_4^+-induced acid load in differentiated Caco-2BBe cells.

Caco-2BBe cells grown on transwell membranes (to allow self-differentiation) for 14 days express the NHE isoforms found in intestinal epithelium *in vivo* [2, 3]. NHE2 displayed the highest mRNA expression levels in these cells, followed by NHE8>NHE3>NHE1. High endogenous NHE2 expression, but low NHE3 expression in Caco 2 cells has been

shown before [19]. Our results show that despite low mRNA expression levels, basolateral acid-activated NHE1 activity was more than six fold higher than apical NHE2, 3 and 8 activities together.

By a combination of pharmacological inhibition and shRNA silencing, NHE2 activity was localized to the apical membrane in the present study, confirming the result of heterologous expression studies in this cell line [19], and those performed in murine colon [5, 6]. The functional activity of NHE2 in the apical membrane was surprisingly low, given the relatively high expression levels compared to the basolateral NHE1. These results correlate with earlier observations for a short life of the protein when rabbit NHE2 was expressed in PS120 fibroblasts [21], and suggest that endogenous human enterocyte NHE2 may also have a short half-life.

Despite the low NHE2-mediated proton flux rates during pH_i-recovery from an acid load (a technique designed to activate all NHEs to near maximal levels), the difference in steady-state pH_i between C2PLKO.1 and C2NHE2KD cells points to a unique role of NHE2 in enterocyte physiology. Given the high expression levels for NBCn1, it is even more surprising that this difference is also seen in the presence of CO_2/HCO_3^-. It may be explained by the fact that NHE2 has a particularly high proton affinity both at the intra- and the extracellular binding site [43]. This allows NHE2 to remain active even at very high intra- and extracellular pH. The fact that even the highly expressed NBCn1 cannot abrogate the pH_i-difference may be related to the high expression of HCO_3^--dependent acid loaders in this cell line, such as SLC26A3 (suppl. Fig. 5).

In native murine intestine, NHE2 mediates equally high proton efflux rates as NHE1 during pH_i recovery from a NH_4^+-induced acid load in enterocytes localized in the lower part of murine colonic crypts [23]. If the NHE2 half-life is similar in the native colonic epithelium as found both for NHE2-transfected fibroblasts and for the endogenous NHE2 of Caco-2BBe cells, the robust cryptal NHE2 functional activity in the base of the colonic crypt would require very high NHE2 expression levels in this part of the crypt. This underlines the potential importance of NHE2 for cellular physiology in this segment of the intestinal epithelium and suggests the existence of unknown mechanisms that stimulate NHE2 transcription in the cryptal epithelium. The prospect of the physiological significance of this question is to be addressed in the future by appropriate techniques such as laser dissection or *in situ* PCR.

Guan *et al.* demonstrated the high apical NHE2 expression in the mid-distal part of the murine colon by immunohistochemistry [5]. They utilized confocal microscopy to measure acid-induced pH_i recovery in muscle-stripped *nhe2*$^{-/-}$ and *wt* distal colonic mucosa in a perfusion chamber, enabling the investigators to individually perfuse the luminal and serosal compartment. Their results in the intact native murine colon agree with the present study in several aspects. Namely, they also demonstrate a higher basolateral than apical NHE activity, although their approach did not quantitatively compare the two, and they also find an upregulation of a Na^+-dependent proton extrusion mechanism in the absence of NHE2 expression that was not sensitive to luminal NHE inhibitors. An advantage of our study is that we were able to measure the expression of the NHEs in the cells that we study

functionally. In contrast, optically focusing on the same plane of enterocytes in the cryptal base of colonic epithelium of *wt* and *slc9a2*$^{-/-}$ mice may result in a different cell type being studied, since the *slc9a2*$^{-/-}$ colonic mucosa displays a disturbed enterocyte differentiation pattern [44].

The filter-based pH-fluorometry in conjunction with the novel inhibitor tenapanor allows the study of the small endogenous NHE3 transport activity in the Caco-2BBe model without the use of isotopes [45]. Previous functional assessment of endogenous NHE3 in Caco-2BBe was mostly performed with $^{22}Na^+$ isotope flux studies. The literature reports substantial inhibition of NHE1 by the best selective NHE3 inhibitor available up to now, the S1611 compound, and we also observed a robust NHE1 inhibition by 10 μM S1611 [31]. The recently developed tenapanor, on the other hand, was found to inhibit selectively NHE3 [26], and our data support this concept. Since heterologous NHE3 expression had a variety of disadvantages, such as the differential regulation of the promotor used for heterologous NHE3 expression compared to the endogenous NHE3 promotor, the possibility to assess the regulation of endogenous NHE3 expression and measure its transport rate is clearly an advantage. The NH_4^+ prepulse technique allows to acid-activate NHE activity and thus study maximal transport capacity rather than transport rates during steady-state conditions, which may be low.

NHE2-silencing caused a small decrease in the percentage of apical acid-activated NHE activity with an NHE2-typical inhibitor profile. However, since NHE8 mRNA was significantly upregulated in NHE2-silenced Caco-2BBe cells, compensation by NHE8, if present in the apical membrane in Caco-2BBe cells, may mask a part of the decrease in apical NHE2 activity. Because NHE2 and NHE8 activity cannot be reliably distinguished, based on the current knowledge of inhibitor sensitivities against NHE8, we were not able to define an exact NHE2-mediated proton extrusion rate. NHE8 was cloned from rat kidney and later immunolocalized to the microvilli membrane and coated pit region of proximal tubule cells [46, 47]. Shortly thereafter, Nakamura et al. localized human NHE8 to the Golgi apparatus and demonstrated that overexpressing NHE8 in COS7 cells dissipated the acidic Golgi pH, suggesting a role of NHE8 in organelle pH-regulation and function [48]. Cell membrane localization of NHE8 was shown in NRK renal cells, which expresses NHE8 but no NHE3, upon incubation in acidic media [49]. Neither the group of Peter Aronson nor we were able to functionally express NHE8 in the membrane of a stably NHE8-expressing heterologous expression system. When we transiently transfected PS120 fibroblasts with the cDNA for rat NHE8 kindly given to us by Hua Xu [50], highly variable (both in the speed and the time of occurrence after Na^+-re-addition) acid-induced Na^+-dependent pH_i recovery was measured, up to 24 h after the transient transfection. However, after stabile selection of NHE8-expressing clones by antibiotic pressure and repeated acid-suicide cycles, no acid-induced NHE activity was detected in the cell membrane, although the cells displayed NHE8 mRNA expression and the protein was detected by Western blot. Therefore, while NHE8 knockout mouse studies provided ample evidence for an important role of NHE8 in gastrointestinal physiology, the observed gastrointestinal pathology could also be secondary to a defect in organelle transport in enterocytes, with secondary effects on transport, mucin dynamics, barrier function, and microbiome composition [51–54]. More work is needed to clarify whether or not NHE8 is expressed in the Caco-2BBe brush border membrane, and

whether NHE8-mediated Na^+/H^+ exchange can be pharmacologically distinguished from NHE2- and NHE3-mediated Na^+/H^+ exchange.

Previous studies have addressed the function and regulation of the apical and basolateral NHE isoforms NHE1, NHE2 and NHE3 in transfected, nonepithelial cell lines such as PS120 and AP-1 cells [55, 56]. In addition, intestinal cell lines including Caco 2 have been previously used to address the issue of NHE-isoform expression [57], as well polarized NHE activity [19, 40, 58–60], with controversial results. Different groups have stated that Caco 2 cells express only NHE1 on the basolateral side [58], but that heterologously expressed NHE2 and NHE3 localize to the apical membrane [19]. Others have found high endogenous NHE3 expression [40] or high endogenous NHE2 expression on the apical side [19]. Certainly, a part of these discrepancies are due to the fact that different Caco 2 clones may display different characteristics in different laboratories. The scientific literature suggests that culture conditions may also change the expression of ion transporters [40, 61]. Due to the variability of the intestinal cell lines, high hopes are attached to the possibility of growing intestinal organoids with the expression pattern of isolated native epithelia with physiological differentiating pattern and ion transporter expression [62]. Despite certain drawbacks, the study of self-differentiating Caco-2BBe, whose gene expression profile closely mimics that of differentiated intestinal enterocytes [63], and whose ion transport characteristics differ from those reported for other cell lines [64, 65], closely mimics those of intestinal organoids during differentiation [66]. For example the observed increase of mRNA expression for absorptive transporters and decrease for secretory transporters during the culture time (suppl. Fig. 5), allows to study enterocyte mRNA expression and polarized function in a purely epithelial preparation with good reproducibility over several decades.

The discrepant results in the literature may also in part be due to the overlapping inhibition curves for NHE1, NHE2 and presumably NHE8 for the currently available inhibitors. While HOE642 has the widest distance between NHE1 and NHE3 inhibition curves, they have been originally described using very low external Na^+ concentrations [24, 67]. When perfusing the human or rat NHE1-expressing PS120 cells with physiological (~140 mM) Na^+ concentrations, we had noticed earlier that 1 μM HOE642, a concentration frequently used to inhibit NHE1, inhibited only ~ 95% of acid-activated NHE1-mediated proton flux. Our NHE2-expressing PS120 cells did not have good/high NHE2 activity, but when we later overexpressed NHE2 in RGM-1 gastric epithelia cells, it became clear that 3 μM HOE642, found to inhibit ~ 99% of rat NHE1, already inhibited ~ 15% of NHE2 activity [31]. This overlap, which is stronger with the use of HOE694 and other NHE inhibitors, probably explains many of the discrepancies related to the relative contribution of different NHE isoforms to a given epithelial proton flux. In order to avoid this problem we used the method of selectively perfusing the apical and basolateral side of the cells with a rapid flow rate, so that the complete lack of Na^+ in one perfusate blocked the activity of all NHE isoforms in the respective membrane. This allowed inhibition of the considerable NHE1 activity in the basolateral membrane without interfering with the modest NHE2, NHE3 and possibly NHE8 activities in the apical membrane.

Conclusion

In summary, this study describes the expression, localization and functional activity of the major NHE isoforms expressed in self-differentiating filter-grown intestinal Caco-2BBe cells. Reproducibility, environmental control, wide availability of the employed methods and elimination of the necessity for radioisotopes increase the attractiveness to study endogenous regulation of intestinal NHE isoforms in a well-differentiated intestinal cell line. Despite much lower transport activity of NHE2 compared to NHE1 at low intracellular pH_i, NHE2 was nevertheless important in the maintenance of the high steady-state pH_i of these cells, likely because of its previously reported uniquely high proton affinity [43]. The Caco-2BBe cell line, which also endogenously expresses all currently known NHERF adaptor protein family members, may be an interesting model to further study the signaling steps involved in the regulation of intestinal NHE isoforms.

Supplementary Material

Refer to Web version on PubMed Central for supplementary material.

Acknowledgements

We gratefully acknowledge receipt of the rNHE3 expression vector from Chung Ming Tse, John Hopkins School of Medicine, Baltimore, the hNHE8 expression vector from Hua Xu, University of Arizona, Tucson.

The project was funded by the Deutsche Forschungsgemeinschaft grants SFB621/C9 and SE460/21-1 (to US), and by a grant from the Volkswagenstiftung VW Vorab (to US).

Y.Y, A.E.S, K. Z, Z.Y, S.Y, M. A., K.N. and U.S. designed, performed and analyzed experiments, C.C.Y supplied important technical resources, Y.Y., K.N., and U.S. wrote the manuscript.

The present addresses of the authors Y.Y, Z. Y and S. Y are the following: [§]Yan Yu: Department of Gastroenterology, Tongji Hospital, Tongji Medical College, Huazhong University of Science and Technology, Wuhan, China, [&]Zhenglin Yuan: Department of Stomatology, Union Hospital, Tongji Medical College, Huazhong University of Science and Technology, Wuhan, China, [%]Sunil Yeruva: Department of Anatomy, Ludwig Maximilians University of Munich, Germany.

References

1. Fuster DG, Alexander RT: Traditional and emerging roles for the SLC9 Na+/H+ exchangers. Pflugers Arch 2014;466:61–76. [PubMed: 24337822]
2. Xu H, Ghishan FK, Kiela PR: SLC9 Gene Family: Function, Expression, and Regulation. Compr Physiol 2018;8:555–583. [PubMed: 29687889]
3. Donowitz M, Ming Tse C, Fuster D: SLC9/NHE gene family, a plasma membrane and organellar family of Na(+)/H(+) exchangers. Mol Aspects Med 2013;34:236–251. [PubMed: 23506868]
4. Wang Z, Orlowski J, Shull GE: Primary structure and functional expression of a novel gastrointestinal isoform of the rat Na/H exchanger. J Biol Chem 1993;268:11925–11928. [PubMed: 7685026]
5. Guan Y, Dong J, Tackett L, Meyer JW, Shull GE, Montrose MH: NHE2 is the main apical NHE in mouse colonic crypts but an alternative Na+-dependent acid extrusion mechanism is upregulated in NHE2-null mice. Am J Physiol Gastrointest Liver Physiol 2006;291:G689–699. [PubMed: 16690903]
6. Chu J, Chu S, Montrose MH: Apical Na+/H+ exchange near the base of mouse colonic crypts. Am J Physiol Cell Physiol 2002;283:C358–372. [PubMed: 12055105]

7. Gawenis LR, Stien X, Shull GE, Schultheis PJ, Woo AL, Walker NM, Clarke LL: Intestinal NaCl transport in NHE2 and NHE3 knockout mice. Am J Physiol Gastrointest Liver Physiol 2002;282:G776–784. [PubMed: 11960774]
8. Xia W, Yu Q, Riederer B, Singh AK, Engelhardt R, Yeruva S, Song P, Tian DA, Soleiman M, Seidler U: The distinct roles of anion transporters Slc26a3 (DRA) and Slc26a6 (PAT-1) in fluid and electrolyte absorption in the murine small intestine. Pflugers Arch 2014;466:1541–1556. [PubMed: 24233434]
9. Gonda T, Maouyo D, Rees SE, Montrose MH: Regulation of intracellular pH gradients by identified Na/H exchanger isoforms and a short-chain fatty acid. Am J Physiol1999;276:G259–270. [PubMed: 9887003]
10. Rajendran VM, Nanda Kumar NS, Tse CM, Binder HJ: Na-H Exchanger Isoform-2 (NHE2) Mediates Butyrate-dependent Na+ Absorption in Dextran Sulfate Sodium (DSS)-induced Colitis. J Biol Chem 2015;290:25487–25496. [PubMed: 26350456]
11. Sellin JH, De Soignie R: Short-chain fatty acids have polarized effects on sodium transport and intracellular pH in rabbit proximal colon. Gastroenterology 1998;114:737–747. [PubMed: 9516394]
12. Musch MW, Bookstein C, Xie Y, Sellin JH, Chang EB: SCFA increase intestinal Na absorption by induction of NHE3 in rat colon and human intestinal C2/bbe cells. Am J Physiol Gastrointest Liver Physiol 2001;280:G687–693. [PubMed: 11254495]
13. Vidyasagar S, Ramakrishna BS: Effects of butyrate on active sodium and chloride transport in rat and rabbit distal colon. J Physiol 2002;539:163–173. [PubMed: 11850510]
14. Lu Z, Yao L, Jiang Z, Aschenbach JR, Martens H, Shen Z: Acidic pH and short-chain fatty acids activate Na+ transport but differentially modulate expression of Na+/H+ exchanger isoforms 1, 2, and 3 in omasal epithelium. J Dairy Sci 2016;99:733–745. [PubMed: 26547645]
15. Gonçalves P, Martel F: Regulation of colonic epithelial butyrate transport: Focus on colorectal cancer. Porto Biomed J 2016;1:83–91. [PubMed: 32258556]
16. Nath SK, Hang CY, Levine SA, Yun CH, Montrose MH, Donowitz M, Tse CM: Hyperosmolarity inhibits the Na+/H+ exchanger isoforms NHE2 and NHE3: an effect opposite to that on NHE1. Am J Physiol 1996;270:G431–441. [PubMed: 8638709]
17. Chow CW, Woodside M, Demaurex N, Yu FH, Plant P, Rotin D, Grinstein S, Orlowski J: Proline-rich motifs of the Na+/H+ exchanger 2 isoform. Binding of Src homology domain 3 and role in apical targeting in epithelia. J Biol Chem 1999;274:10481–10488. [PubMed: 10187839]
18. Soleimani M, Singh G, Bizal GL, Gullans SR, McAteer JA: Na+/H+ exchanger isoforms NHE-2 and NHE-1 in inner medullary collecting duct cells. Expression, functional localization, and differential regulation. J Biol Chem 1994;269:27973–27978. [PubMed: 7961730]
19. McSwine RL, Musch MW, Bookstein C, Xie Y, Rao M, Chang EB: Regulation of apical membrane Na+/H+ exchangers NHE2 and NHE3 in intestinal epithelial cell line C2/bbe. Am J Physiol 1998;275:C693–701. [PubMed: 9730953]
20. Chow CW: Regulation and intracellular localization of the epithelial isoforms of the Na+/H+ exchangers NHE2 and NHE3. Clin Invest Med 1999;22:195–206. [PubMed: 10579058]
21. Cavet ME, Akhter S, Murtazina R, Sanchez de Medina F, Tse CM, Donowitz M: Half-lives of plasma membrane Na(+)/H(+) exchangers NHE1–3: plasma membrane NHE2 has a rapid rate of degradation. Am J Physiol Cell Physiol 2001;281:C2039–2048. [PubMed: 11698263]
22. Yoo BK, Yanda MK, No YR, Yun CC: Human intestinal epithelial cell line SK-CO15 is a new model system to study Na(+)/H(+) exchanger 3. Am J Physiol Gastrointest Liver Physiol 2012;303:G180–188. [PubMed: 22556145]
23. Bachmann O, Riederer B, Rossmann H, Groos S, Schultheis PJ, Shull GE, Gregor M, Manns MP, Seidler U: The Na+/H+ exchanger isoform 2 is the predominant NHE isoform in murine colonic crypts and its lack causes NHE3 upregulation. Am J Physiol Gastrointest Liver Physiol 2004;287:G125–133. [PubMed: 14962844]
24. Scholz W, Albus U, Counillon L, Gogelein H, Lang HJ, Linz W, Weichert A, Scholkens BA: Protective effects of HOE642, a selective sodium-hydrogen exchange subtype 1 inhibitor, on cardiac ischaemia and reperfusion. Cardiovasc Res 1995;29:260–268. [PubMed: 7736504]

25. Baumgarth M, Beier N, Gericke R: (2-Methyl-5-(methylsulfonyl)benzoyl)guanidine Na+/H+ antiporter inhibitors. J Med Chem 1997;40:2017–2034. [PubMed: 9207943]
26. Spencer AG, Labonte ED, Rosenbaum DP, Plato CF, Carreras CW, Leadbetter MR, Kozuka K, Kohler J, Koo-McCoy S, He L, Bell N, Tabora J, Joly KM, Navre M, Jacobs JW, Charmot D: Intestinal inhibition of the Na+/H+ exchanger 3 prevents cardiorenal damage in rats and inhibits Na+ uptake in humans. Sci Transl Med 2014;6:227ra236.
27. He P, Zhang H, Yun CC: IRBIT, inositol 1, 4,5-triphosphate (IP3) receptor-binding protein released with IP3, binds Na+/H+ exchanger NHE3 and activates NHE3 activity in response to calcium. J Biol Chem 2008;283:33544–33553. [PubMed: 18829453]
28. Yeruva S, Chodisetti G, Luo M, Chen M, Cinar A, Ludolph L, Lünnemann M, Goldstein J, Singh AK, Riederer B, Bachmann O, Bleich A, Gereke M, Bruder D, Hagen S, He P, Yun C, Seidler U: Evidence for a causal link between adaptor protein PDZK1 downregulation and Na(+)/H(+) exchanger NHE3 dysfunction in human and murine colitis. Pflugers Archiv 2015;467:1795–1807. [PubMed: 25271043]
29. Ozkan P, Mutharasan R: A rapid method for measuring intracellular pH using BCECF-AM. Biochim Biophys Acta 2002;1572:143–148. [PubMed: 12204343]
30. Rossmann H, Sonnentag T, Heinzmann A, Seidler B, Bachmann O, Vieillard-Baron D, Gregor M, Seidler U: Differential expression and regulation of Na(+)/H(+) exchanger isoforms in rabbit parietal and mucous cells. Am J Physiol Gastrointest Liver Physiol 2001;281:G447–458. [PubMed: 11447025]
31. Paehler Vor der Nolte A, Chodisetti G, Yuan Z, Busch F, Riederer B, Luo M, Yu Y, Menon MB, Schneider A, Stripecke R, Nikolovska K, Yeruva S, Seidler U: Na(+) /H(+) exchanger NHE1 and NHE2 have opposite effects on migration velocity in rat gastric surface cells. J Cell Physiol 2017;232:1669–1680. [PubMed: 28019659]
32. Cinar A, Chen M, Riederer B, Bachmann O, Wiemann M, Manns M, Kocher O, Seidler U: NHE3 inhibition by cAMP and Ca2+ is abolished in PDZ-domain protein PDZK1-deficient murine enterocytes. J Physiol 2007;581:1235–1246. [PubMed: 17395628]
33. Orlowski J, Kandasamy RA, Shull GE: Molecular cloning of putative members of the Na/H exchanger gene family. cDNA cloning, deduced amino acid sequence, and mRNA tissue expression of the rat Na/H exchanger NHE-1 and two structurally related proteins. J Biol Chem 1992;267:9331–9339. [PubMed: 1577762]
34. Bookstein C, Xie Y, Rabenau K, Musch MW, McSwine RL, Rao MC, Chang EB: Tissue distribution of Na+/H+ exchanger isoforms NHE2 and NHE4 in rat intestine and kidney. Am J Physiol 1997;273:C1496–1505. [PubMed: 9374634]
35. Gawenis LR, Greeb JM, Prasad V, Grisham C, Sanford LP, Doetschman T, Andringa A, Miller ML, Shull GE: Impaired gastric acid secretion in mice with a targeted disruption of the NHE4 Na+/H+ exchanger. J Biol Chem 2005;280:12781–12789. [PubMed: 15684419]
36. Bourgeois S, Meer LV, Wootla B, Bloch-Faure M, Chambrey R, Shull GE, Gawenis LR, Houillier P: NHE4 is critical for the renal handling of ammonia in rodents. J Clin Invest 2010;120:1895–1904. [PubMed: 20484819]
37. Beltran AR, Ramirez MA, Carraro-Lacroix LR, Hiraki Y, Reboucas NA, Malnic G: NHE1, NHE2, and NHE4 contribute to regulation of cell pH in T84 colon cancer cells. Pflugers Arch 2008;455:799–810. [PubMed: 17943310]
38. Arena EA, Longo WE, Roberts KE, Geibel P, Nateqi J, Brandstetter M, Geibel JP: Functional role of NHE4 as a pH regulator in rat and human colonic crypts. Am J Physiol Cell Physiol 2012;302:C412–418. [PubMed: 22049213]
39. Magro F, Fraga S, Soares-da-Silva P: Signaling of short- and long-term regulation of intestinal epithelial type 1 Na+/H+ exchanger by interferon-gamma. Br J Pharmacol 2005;145:93–103. [PubMed: 15723092]
40. Janecki AJ, Montrose MH, Tse CM, de Medina FS, Zweibaum A, Donowitz M: Development of an endogenous epithelial Na(+)/H(+) exchanger (NHE3) in three clones of caco-2 cells. Am J Physiol 1999;277:G292–305. [PubMed: 10444443]

41. Praetorius J, Kim YH, Bouzinova EV, Frische S, Rojek A, Aalkjaer C, Nielsen S: NBCn1 is a basolateral Na+-HCO3- cotransporter in rat kidney inner medullary collecting ducts. Am J Physiol Renal Physiol 2004;286:F903–912. [PubMed: 15075186]

42. Aalkjaer C, Boedtkjer E, Choi I, Lee S: Cation-coupled bicarbonate transporters. Compr Physiol 2014;4:1605–1637. [PubMed: 25428855]

43. Yu FH, Shull GE, Orlowski J: Functional properties of the rat Na/H exchanger NHE-2 isoform expressed in Na/H exchanger-deficient Chinese hamster ovary cells. J Biol Chem 1993;268:25536–25541. [PubMed: 8244989]

44. Nikolovska K, Li C, Yu Y, Yuan Z, Seidler A, Kini A, Yeruva S, Singh AK, Riederer B, Seidler U: The Sodium/Hydrogen Exchanger 2 (Slc9a2/NHE2) is Involved in the Differentiation of Colonic Intestinal Epithelial Cells. FASEB J 2018;32:747.15–747.15.

45. Bookstein C, Musch MW, Xie Y, Rao MC, Chang EB: Regulation of Intestinal Epithelial Brush Border Na+/H+ Exchanger Isoforms, NHE2 and NHE3, in C2bbe Cells. J Membr Biol 1999;171:87–95. [PubMed: 10485997]

46. Goyal S, Mentone S, Aronson PS: Immunolocalization of NHE8 in rat kidney. Am J Physiol Renal Physiol 2005;288:F530–538. [PubMed: 15522984]

47. Goyal S, Vanden Heuvel G, Aronson PS: Renal expression of novel Na+/H+ exchanger isoform NHE8. Am J Physiol Renal Physiol 2003;284:F467–473. [PubMed: 12409279]

48. Nakamura N, Tanaka S, Teko Y, Mitsui K, Kanazawa H: Four Na+/H+ exchanger isoforms are distributed to Golgi and post-Golgi compartments and are involved in organelle pH regulation. J Biol Chem 2005;280:1561–1572. [PubMed: 15522866]

49. Joseph C, Twombley K, Gattineni J, Zhang Q, Dwarakanath V, Baum M: Acid increases NHE8 surface expression and activity in NRK cells. Am J Physiol Renal Physiol 2012;302:F495–503. [PubMed: 22088432]

50. Xu H, Chen H, Dong J, Lynch R, Ghishan FK: Gastrointestinal Distribution and Kinetic Characterization of the Sodium-Hydrogen Exchanger Isoform 8 (NHE8). Cell Physiol Biochem 2008;21:109–116. [PubMed: 18209477]

51. Xu H, Zhang B, Li J, Wang C, Chen H, Ghishan FK: Impaired mucin synthesis and bicarbonate secretion in the colon of NHE8 knockout mice. Am J Physiol Gastrointest Liver Physiol 2012;303:G335–343. [PubMed: 22575219]

52. Wang A, Li J, Zhao Y, Johansson ME, Xu H, Ghishan FK: Loss of NHE8 expression impairs intestinal mucosal integrity. Am J Physiol Gastrointest Liver Physiol 2015;309:G855–864. [PubMed: 26505975]

53. Liu C, Xu H, Zhang B, Johansson ME, Li J, Hansson GC, Ghishan FK: NHE8 plays an important role in mucosal protection via its effect on bacterial adhesion. Am J Physiol Cell Physiol 2013;305:C121–128. [PubMed: 23657568]

54. Xu H, Li J, Chen H, Wang C, Ghishan FK: NHE8 plays important roles in gastric mucosal protection. Am J Physiol Gastrointest Liver Physiol 2013;304:G257–261. [PubMed: 23220221]

55. Kapus A, Grinstein S, Wasan S, Kandasamy R, Orlowski J: Functional characterization of three isoforms of the Na+/H+ exchanger stably expressed in Chinese hamster ovary cells. ATP dependence, osmotic sensitivity, and role in cell proliferation. J Biol Chem 1994;269:23544–23552. [PubMed: 8089122]

56. Levine SA, Montrose MH, Tse CM, Donowitz M: Kinetics and regulation of three cloned mammalian Na+/H+ exchangers stably expressed in a fibroblast cell line. J Biol Chem 1993;268:25527–25535. [PubMed: 8244988]

57. Alrefai WA, Scaglione-Sewell B, Tyagi S, Wartman L, Brasitus TA, Ramaswamy K, Dudeja PK: Differential regulation of the expression of Na(+)/H(+) exchanger isoform NHE3 by PKC-alpha in Caco-2 cells. Am J Physiol Cell Physiol 2001;281:C1551–1558. [PubMed: 11600418]

58. Watson AJ, Levine S, Donowitz M, Montrose MH: Kinetics and regulation of a polarized Na(+)-H+ exchanger from Caco-2 cells, a human intestinal cell line. Am J Physiol 1991;261:G229–238. [PubMed: 1651659]

59. Tse CM, Levine SA, Yun CH, Montrose MH, Little PJ, Pouyssegur J, Donowitz M: Cloning and expression of a rabbit cDNA encoding a serum-activated ethylisopropylamiloride-resistant

epithelial Na+/H+ exchanger isoform (NHE-2). J Biol Chem 1993;268:11917–11924. [PubMed: 7685025]

60. Toriano R, Ozu M, Politi MT, Dorr RA, Curto MA, Capurro C: Uroguanylin regulates net fluid secretion via the NHE2 isoform of the Na/H+ exchanger in an intestinal cellular model. Cell Physiol Biochem 2011;28:733–742. [PubMed: 22178885]
61. Zucco F, Batto AF, Bises G, Chambaz J, Chiusolo A, Consalvo R, Cross H, Dal Negro G, de Angelis I, Fabre G, Guillou F, Hoffman S, Laplanche L, Morel E, Pincon-Raymond M, Prieto P, Turco L, Ranaldi G, Rousset M, Sambuy Y et al. : An inter-laboratory study to evaluate the effects of medium composition on the differentiation and barrier function of Caco-2 cell lines. Altern Lab Anim 2005;33:603–618. [PubMed: 16372835]
62. Yu H, Hasan NM, In JG, Estes MK, Kovbasnjuk O, Zachos NC, Donowitz M: The Contributions of Human Mini-Intestines to the Study of Intestinal Physiology and Pathophysiology. Annu Rev Physiol 2017;79:291–312. [PubMed: 28192061]
63. Saaf AM, Halbleib JM, Chen X, Yuen ST, Leung SY, Nelson WJ, Brown PO: Parallels between global transcriptional programs of polarizing Caco-2 intestinal epithelial cells *in vitro* and gene expression programs in normal colon and colon cancer. Mol Biol Cell 2007;18:4245–4260. [PubMed: 17699589]
64. Buchwald M, Sood R, Auerbach W: Regulation of expression of CFTR in human intestinal epithelial cells. Adv Exp Med Biol 1991;290:241–250; discussion 250–252. [PubMed: 1719762]
65. Sood R, Bear C, Auerbach W, Reyes E, Jensen T, Kartner N, Riordan JR, Buchwald M: Regulation of CFTR expression and function during differentiation of intestinal epithelial cells. EMBO J 1992;11:2487–2494. [PubMed: 1378393]
66. Yin J, Tse CM, Avula LR, Singh V, Foulke-Abel J, de Jonge HR, Donowitz M: Molecular Basis and Differentiation-Associated Alterations of Anion Secretion in Human Duodenal Enteroid Monolayers. Cell Mol Gastroenterol Hepatol 2018;5:591–609. [PubMed: 29930980]
67. Counillon L, Scholz W, Lang HJ, Pouyssegur J: Pharmacological characterization of stably transfected Na+/ H+ antiporter isoforms using amiloride analogs and a new inhibitor exhibiting anti-ischemic properties. Mol Pharmacol 1993;44:1041–1045. [PubMed: 8246907]
68. Noble RA, Bell N, Blair H, Sikka A, Thomas H, Phillips N, Nakjang S, Miwa S, Crossland R, Rand V, Televantou D, Long A, Keun HC, Bacon CM, Bomken S, Critchlow SE, Wedge SR: Inhibition of monocarboxyate transporter 1 by AZD3965 as a novel therapeutic approach for diffuse large B-cell lymphoma and Burkitt lymphoma. Haematologica 2017;102:1247–1257. [PubMed: 28385782]

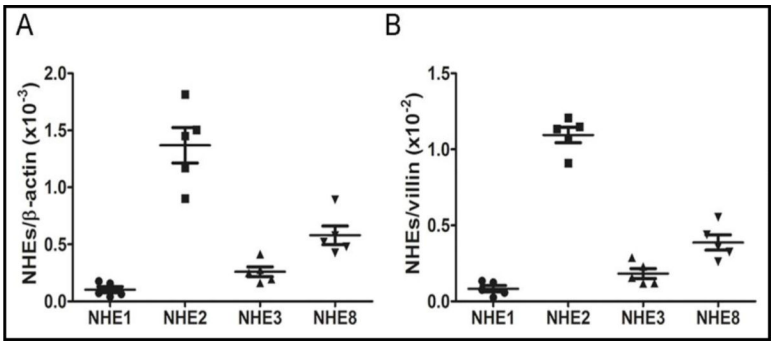

Fig. 1.

NHE mRNA expression levels in Caco-2BBe cells. Real time PCR was utilized to examine the mRNA expression of NHE1, NHE2, NHE3 and NHE8 in differentiated Caco-2BBe cells using β-actin (A) and villin (B) as the reference genes (n=5, mean ± SEM).

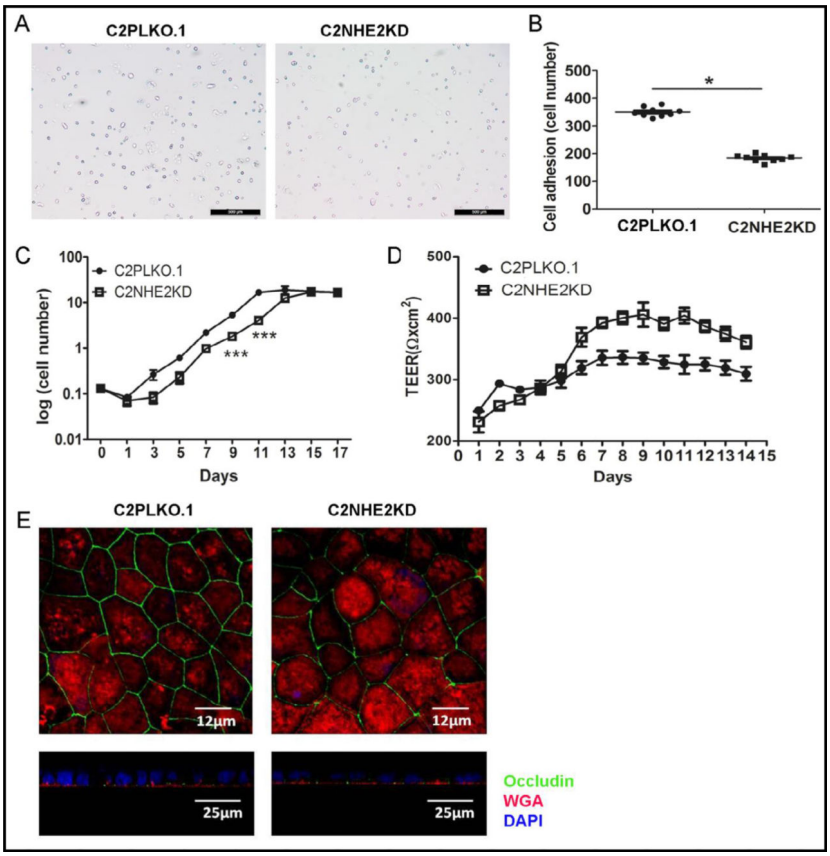

Fig. 2.

Cell characteristics of C2PLKO.1 and C2N2KD cells. (A,B) Cell adhesion of C2PLKO.1 and C2N2KD cells analyzed by counting the adherent cells, 24 h after the cells were seeded with same density. Images of C2PLKO.1 and C2NHE2KD cells were acquired under the phase contrast microscopy. (n=5, mean ± SEM, unpaired student t-test, *p<0.05). (C) The growth curves of C2PLKO.1 cells and C2NHE2KD cells seeded at same density and counted every 48 h. (n=5, mean ± SEM, unpaired student t-test, ***p<0.001) (D) TEER curves of C2PLKO.1 cells and C2NHE2KD cells grown on transwell membranes from day 0 to day 14. (E) Immunofluorescence images of C2PLKO.1 and C2NHE2KD cells on transwell membrane on day 14 in xyz mode (63 ×objective, zoom = 4, scale bar = 12 µm) and in xzy mode (40 × objective, zoom = 3, scale bar = 25 µm). Green occludin, red WGA, blue nucleus. The differences in occludin and WGA immunofluenscence may be due to the difference in height, because the same distance from the support was chosen for the confocal plane. (n = 5, from 3 different cell passages).

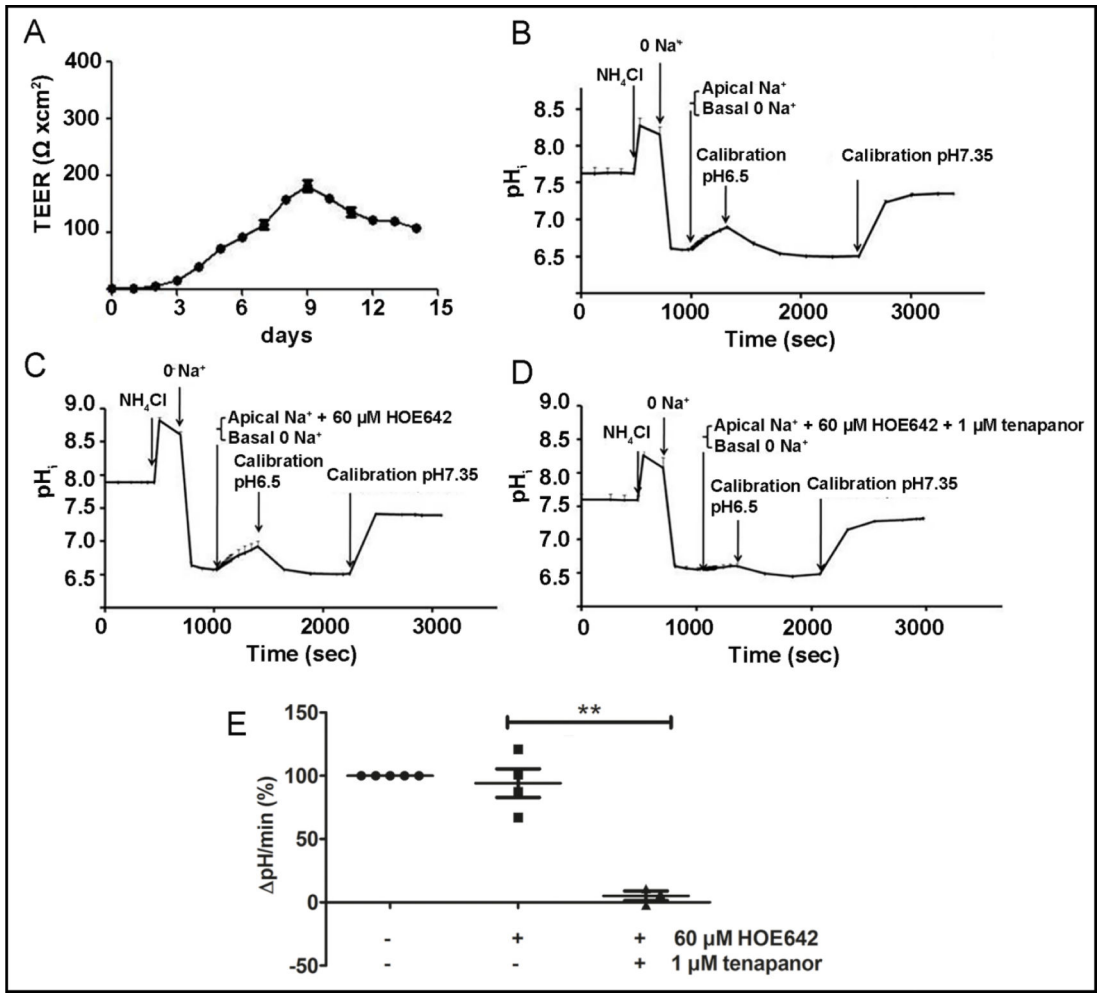

Fig. 3.

Apical Na^+/H^+ exchange rates in NHE3-expressing Caco-2BBe cells are sensitive to tenapanor. (A) TEER curve of hNHE3vsv expressing Caco-2BBe cells after 5 acid suicide selection cycles on transwell membranes from day 0 to day 14 after seeding. (B-D) The NHE function was estimated by first using NH_4Cl prepulse followed by Na^+ free buffer C to cause intracellular acidification, and then Na^+ was added selectively to the apical side during the recovery phase to stimulate apical NHE activity. Inhibitors were added 5 minutes before the addition of Na^+. (B) pH_i curve of total apical NHE activity of C2NHE3vsv AS5 cells. (C) pH_i curve of apical NHE activity in the presence of 60 μM HOE642 in the apical solution. (D) pH_i curve in the presence of 60 μM HOE642 and 1 μM tenapanor in the apical solution. (E) Comparisons of apical NHE activities of C2NHE3vsv cells under different inhibitory conditions. (n=3, mean ± SEM, one-way ANOVA with Tukey's multiple comparison tests, **p<0.001).

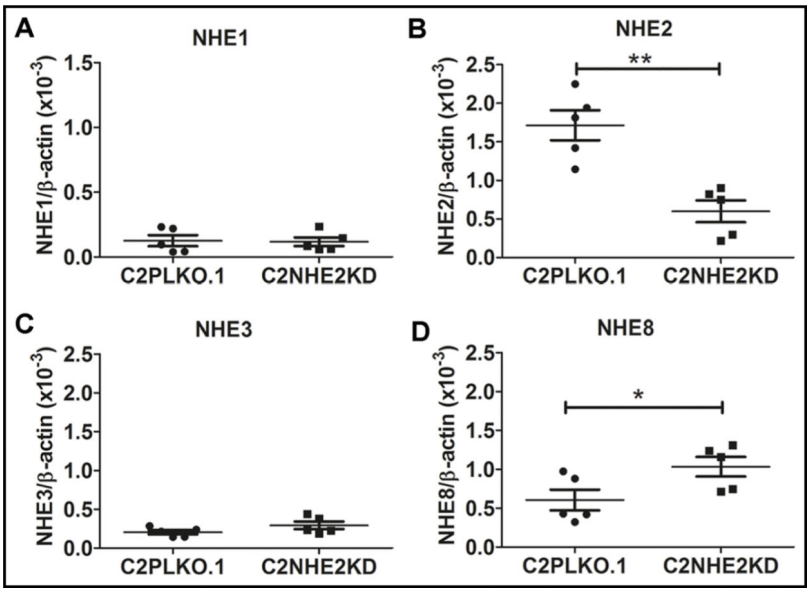

Fig. 4.

mRNA expression of NHE1–3 and NHE8 in 14 day-differentiated, filter-grown Caco-2BBe, C2PLKO.1 and C2NHE2KD cells. Comparisons of (A) NHE1, (B) NHE2, (C) NHE3 and (D) NHE8 mRNA expression levels between C2PLKO.1 and C2NHE2KD cells using β-actin as control gene. (n=5, mean ± SEM, unpaired student t-test, *p<0.05, **p< 0.01).

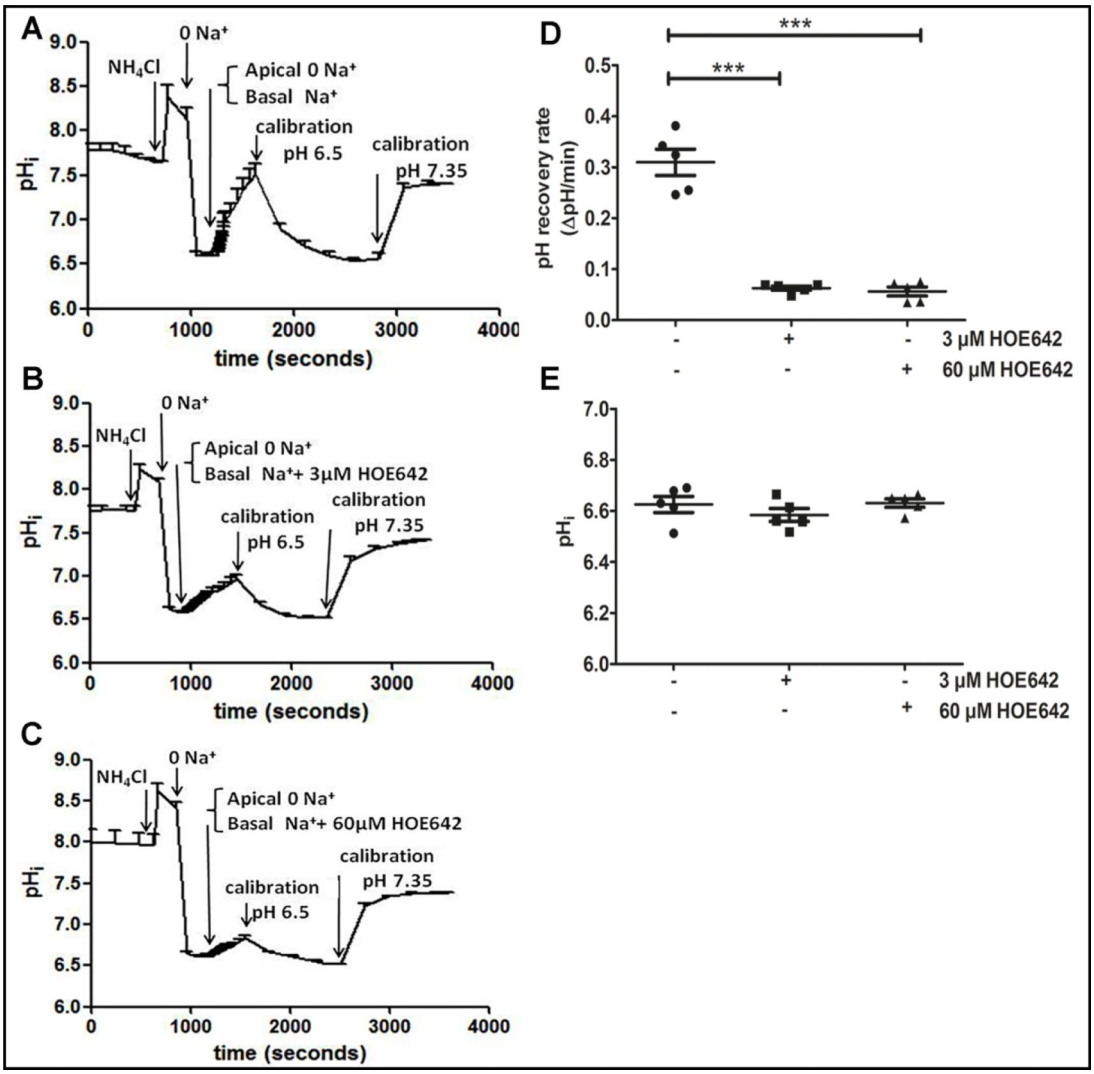

Fig. 5.

Acid-activated basolateral Na^+/H^+ exchange rates in differentiated C2PLKO.1 cells. C2PLKO.1 cells were acidified with the NH_3/NH_4^+ pre-pulse technique. During the recovery phase, the basal side of the cell monolayer was perfused with Na^+-containing buffer A, while the apical side with Na^+-free buffer C. Inhibitors were added 5 minutes before pH_i recovery. (A) pH_i curve of basolateral pH_i recovery without inhibitors, (B) in the presence of 3 μM HOE642, (C) in the presence of 60 μM HOE642 in the basal perfusate in C2PLKO.1 cells. (D) comparisons of acid-activated basolateral Na^+/H^+ exchange rates without inhibition and after 3 μM HOE642 and 60 μM HOE642 treatments. The total basolateral Na^+/H^+ exchange rate of C2PLKO.1 cells was 0.310 ± 0.026 (ΔpH/min). 3 μM HOE642 reduced acid-activated basolateral Na^+/H^+ exchange rates to 0.063 ± 0.004 (ΔpH/min), and 60 μM HOE 642 to 0.056 ± 0.009 (ΔpH/min). (E) Comparisons of initial pH_i at the beginning of acid-induced pH_i recovery among different groups. (n=5, mean ± SEM, one-way ANOVA with Tukey's multiple comparison tests, ***$p < 0.0001$).

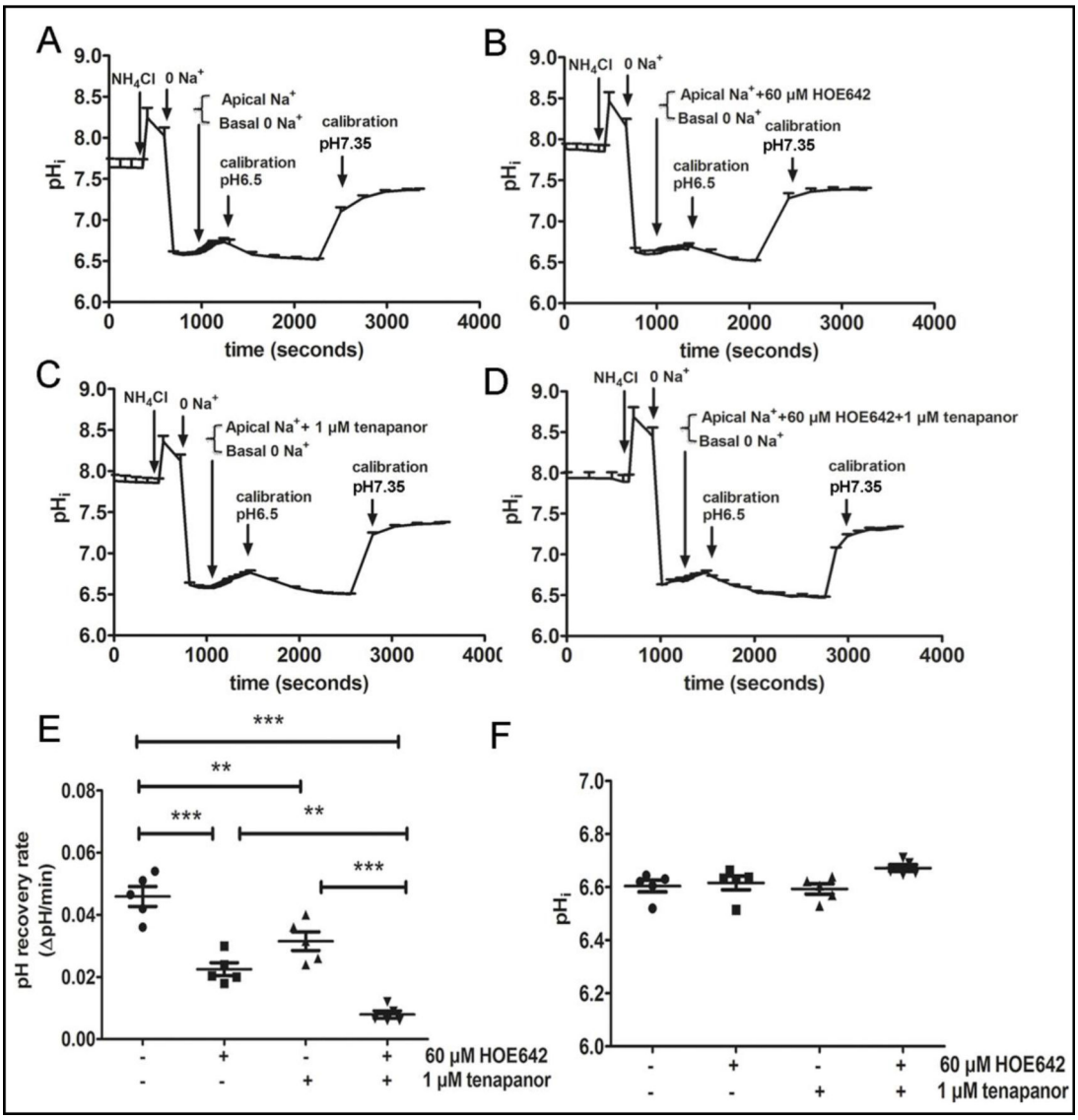

Fig. 6.

Acid-activated apical Na^+/H^+ exchange rates in differentiated C2PLKO.1 cells. In these experiments, the apical side of the cell monolayer was perfused with Na^+-containing buffer A, while the basal side with Na^+-free buffer C during the pH_i-recovery period. (A) pH_i curve of apical pH_i recovery in the absence of inhibitors, (B) in the presence of 60 μM HOE642, (C) in the presence of 1 μM tenapanor, (D) in the presence of 60 μM HOE642 and 1 μM tenapanor in the apical perfusate in C2PLKO.1 cells. (E) comparisons of acid-activated apical Na^+/H^+ exchange rates without inhibitors, with 60 μM HOE642, 1 μM tenapanor, and 60 μM HOE642 plus 1 μM tenapanor. The total apical Na^+/H^+ exchange rate of C2PLKO.1 cells was 0.046 ± 0.003 (ΔpH/min). 60 μM HOE642 reduced acid-activated apical Na^+/H^+ exchange rates to 0.022 ±0.002 (ΔpH/min), 1 μM tenapanor to 0.032 ± 0.003 (ΔpH/min), and 60 μM HOE642 plus 1 μM tenapanor to 0.008 ± 0.001 (ΔpH/min). (F) Comparisons of initial pH_i at the beginning of acid-induced pH_i recovery among different

groups. (n=5, mean ± SEM, one-way ANOVA with Tukey's multiple comparison tests, **p< 0.01, ***p<0.0001).

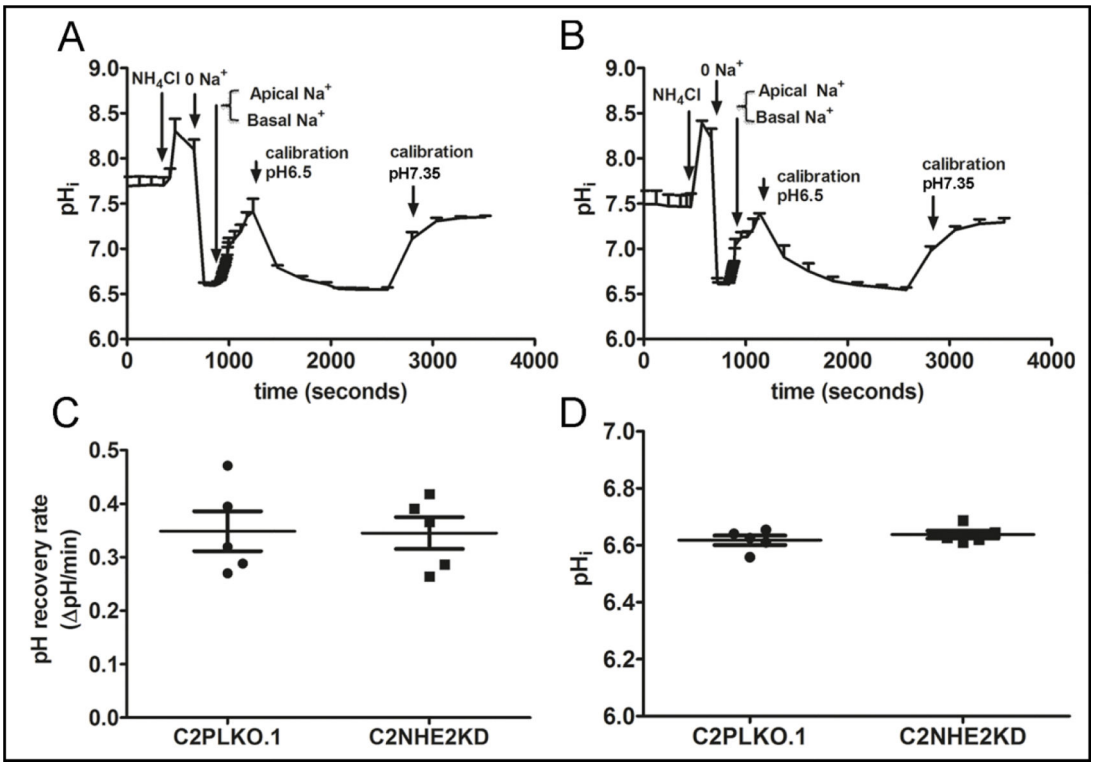

Fig. 7.

Acid-activated total Na^+/H^+ exchange rates in differentiated C2PLKO.1 andC2NHE2KD cells. Both apical and basal sides of the cell monolayer were perfused with Na^+-containing solution without inhibitors. (A) pH_i recovery curve in C2PLKO.1 cells, (B) in C2NHE2KD cells. (C) Comparison of acid-activated Na^+/H^+ exchange rates in C2PLKO.1 and C2NHE2KD cells. (D) Comparison of initial pH_i at the beginning of acid-induced pH_i recovery. (n=5, mean ± SEM).

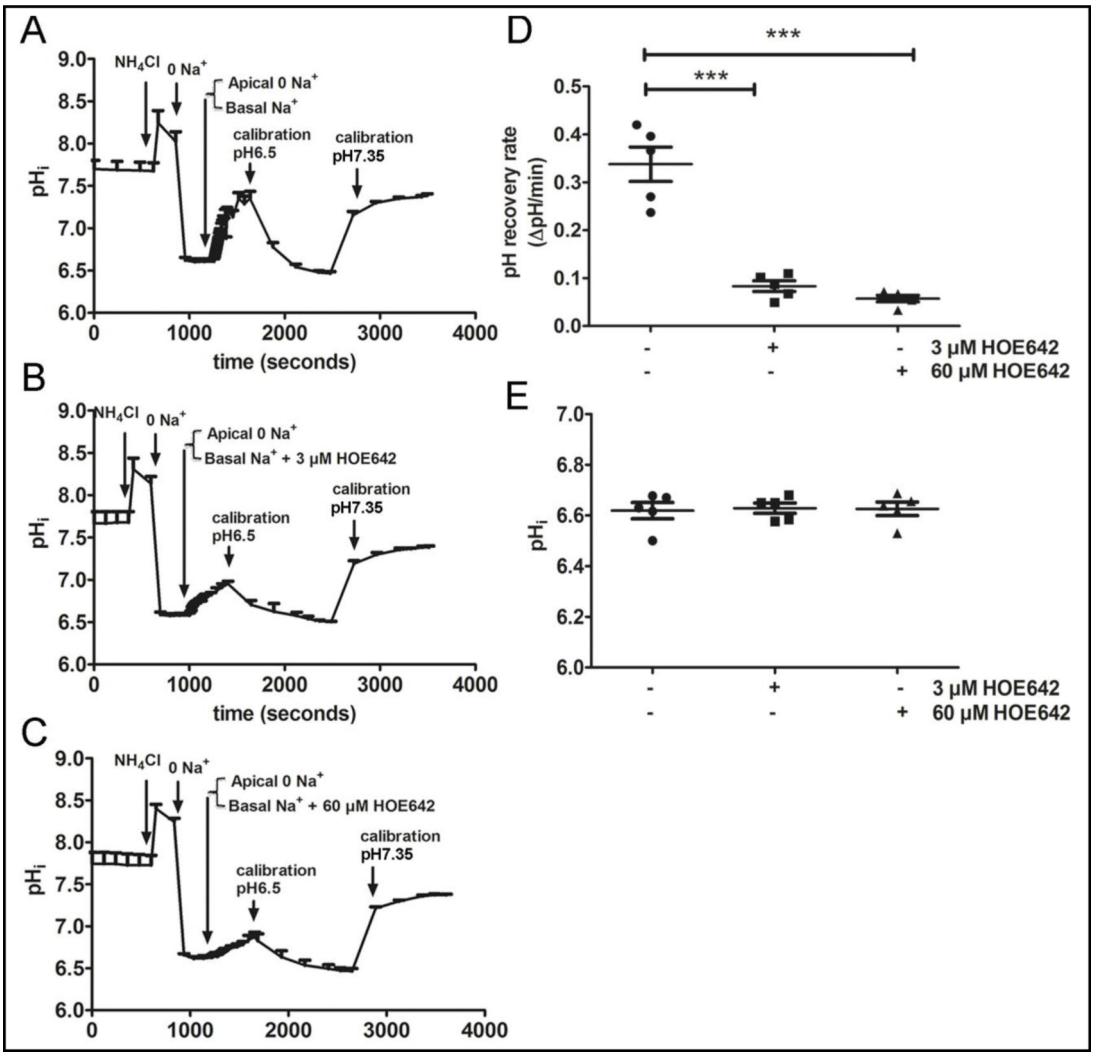

Fig. 8.

Acid-activated basolateral Na^+/H^+ exchange rates in differentiated C2NHE2KD cells. The experimental design and solutions were identical to those in Fig. 5. (A) pH_i-curve of C2NHE2KD without inhibitors, (B) in the presence of 3 μM HOE642, (C) in the presence of 60 μM HOE642. (D) Comparisons of acid-induced pH_i recovery rates under control, 3 μM HOE642 and 60 μM HOE642 treatments in C2NHE2KD cells. The acid-activated total basal Na^+/H^+ exchange rates in C2NHE2KD cells was 0.34 ± 0.036 (ΔpH/min). 3 μM HOE642 reduced this rate to 0.083 ± 0.011 (ΔpH/min). 60 μM HOE642 reduced this rate to 0.057 ± 0.007 (ΔpH/min). (E) Comparisons of initial pH_i at the beginning of pH_i recovery under control, 3 μM HOE642 and 60 μM HOE642 treatments in C2NHE2KD cells. (n=5, mean ± SEM, one-way ANOVA with Tukey's multiple comparison tests, ***p<0.0001).

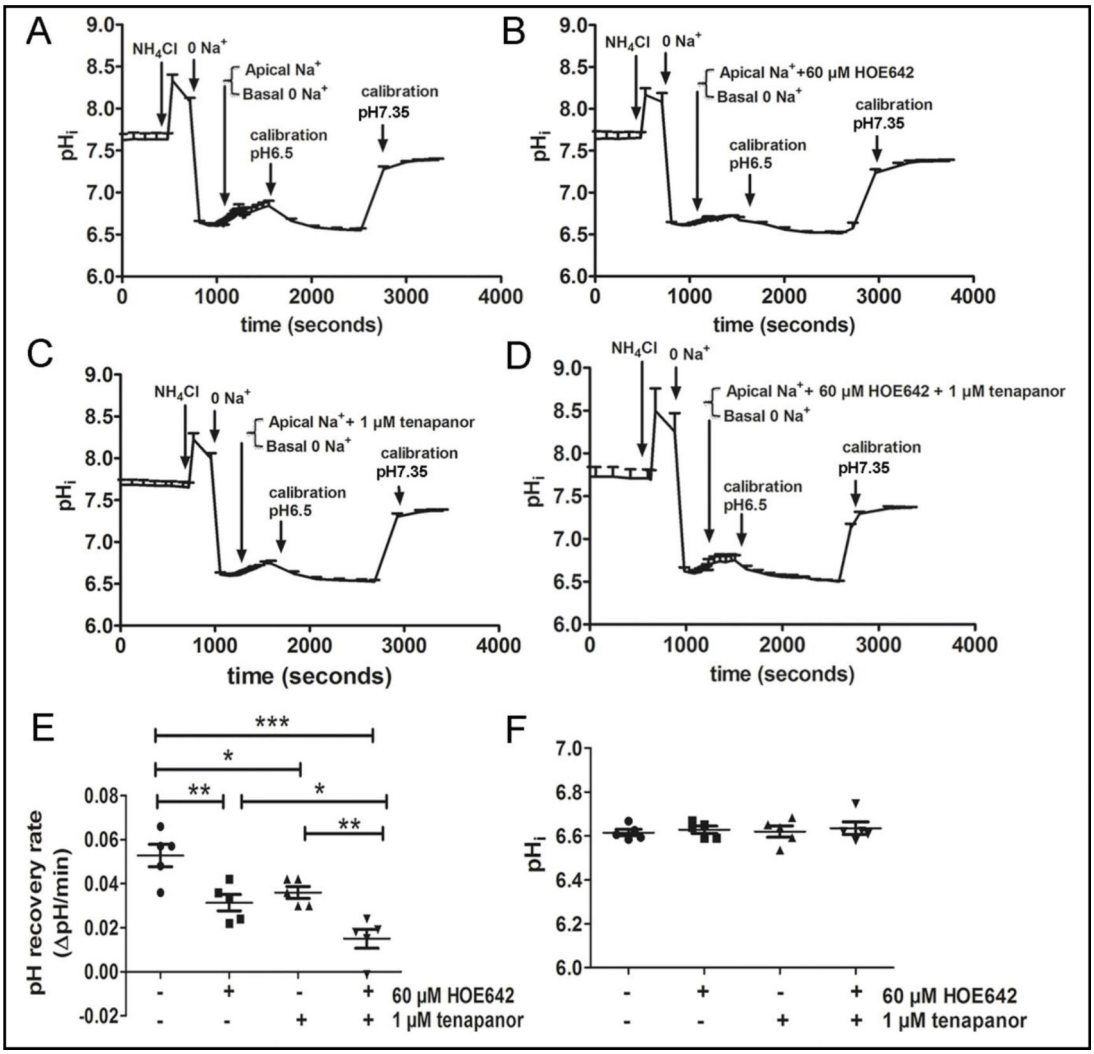

Fig. 9.

Acid-activated apical Na^+/H^+ exchange rates in differentiated C2NHE2KD cells. The experimental design, solutions and inhibitors were the same as in Fig. 6. (A) pH_i-recovery curve without inhibitors, (B) in the presence of 60 μM HOE642, (C) in the presence of 1 μM tenapanor, (D) in the presence of 60 μM HOE642 and 1 μM tenapanor during apical Na^+ re-addition in C2NHE2KD cells. (E) Comparisons of acid-activated apical Na^+/H^+ exchange rates under control, 60 μM HOE642, 1 μM tenapanor, and 60 μM HOE642 plus 1 μM tenapanor. The total apical Na^+/H^+ exchange rate of C2NHE2KD cells was 0.050 ± 0.005 (ΔpH/min). 60 μM HOE642 reduced acid-activated apical Na^+/H^+ exchange rate to 0.031 ±0.004 (ΔpH/min), 1 μM tenapanor to 0.036 ± 0.003 (ΔpH/min) and 60 μM HOE642 plus 1μM tenapanor to 0.015 ± 0.004 (ΔpH/min). (F) Comparisons of initial pH_i at the beginning of acid-induced pH_i recovery among different groups. (n=5, mean ± SEM, one-way ANOVA with Tukey's multiple comparison tests, *p< 0.05, **p< 0.001, ***p< 0.0001).

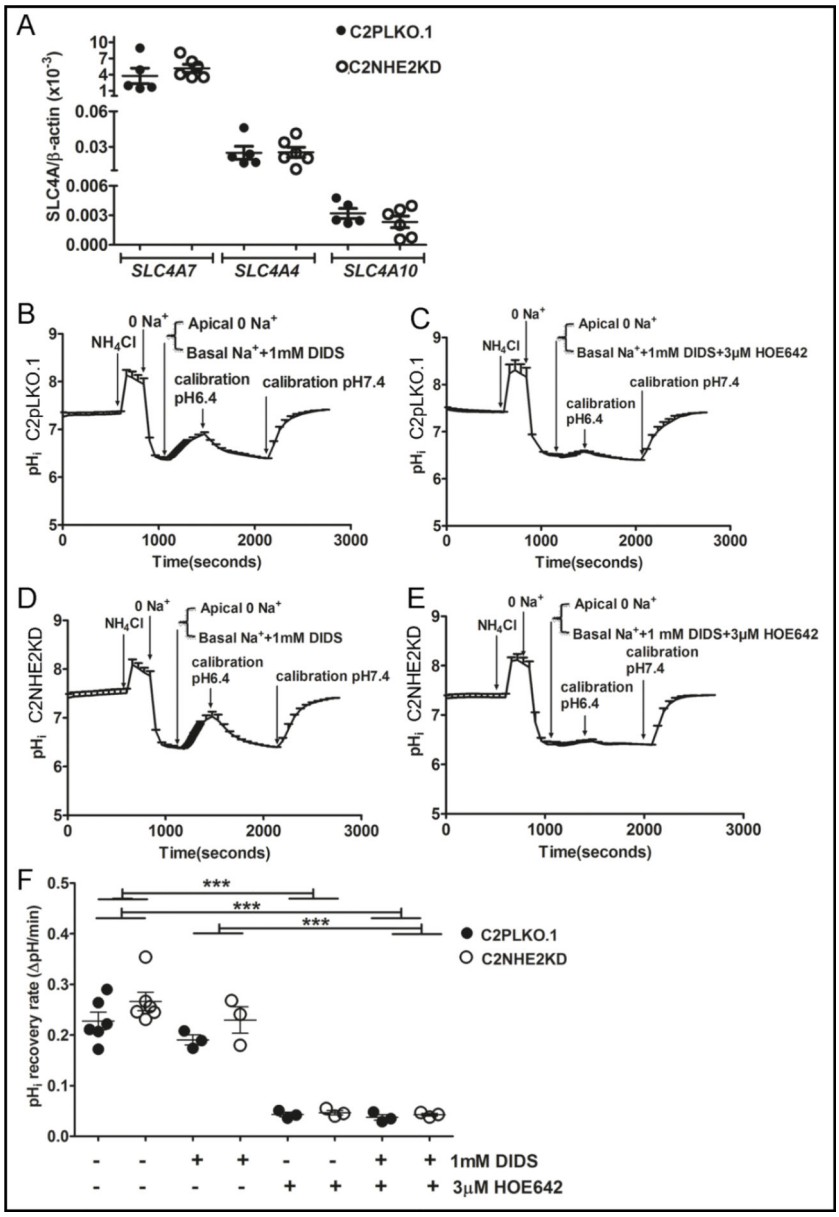

Fig. 10.

mRNA expression of SLC4A7, 4 and 10 and acid-activated basolateral Na+/H+ exchange after DIDS treatment of differentiated cells. (A) Comparisons of SLC4A7, SLC4A4 and SLC4A10 mRNA expression levels between differentiated C2PLKO.1 (●) and C2NHE2KD (○) cells using β-actin as control gene. (n=5–6, mean ± SEM). Acid-activated basolateral Na^+/H^+ exchange after DIDS treatment of differentiated cells was performed as described in Fig. 5. and 8. Inhibitors were added 5 minutes before pH_i recovery. pH_i-curve of (B) C2PLKO.1 and (C) C2NHE2KD in the presence of 1 mM DIDS. pH_i-curve of (D) C2PLKO.1 and (E) C2NHE2KD in the presence of 1 mM DIDS plus 3 μM HOE642, (F) comparisons of acid-induced pH_i recovery rates between control, 1 mM DIDS, 3 μM HOE642 and 1 mM DIDS plus 3 μM HOE642 treatments in C2PLKO.1 (●) and C2NHE2KD (○) cells. No differences in the acid-activated basal Na^+/H^+ exchange rates

were observed among control and DIDS perfused cells, regardless of the cell genotype. Co-perfusion with 3 μM HOE642 plus 1 mM DIDS reduced this rate to the level of only 3 μM HOE642 perfused cells in both C2PLKO.1 and C2NHE2KD cells (n=3–6, mean ± SEM, one-way ANOVA with Tukey's multiple comparison tests, ***p<0.0001).

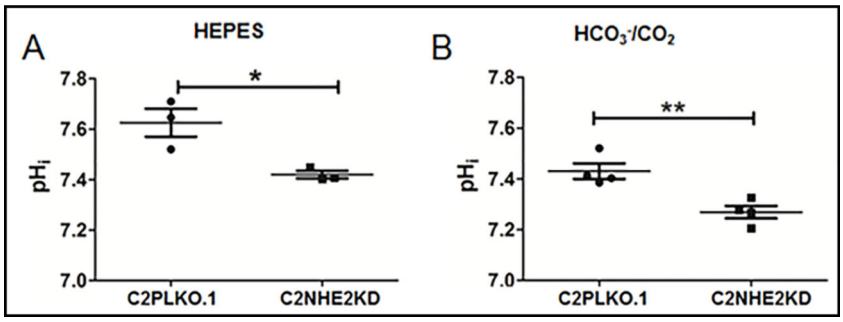

Fig. 11.

Steady-state pH_i of C2PLKO.1 and C2NHE2KD cells. (A) steady-state pH_i values of C2PLKO.1 and C2NHE2KD cells measured during perfusion with HEPES buffer followed by calibration with pH6.5 and pH7.0 solution gassed with O_2. (B) steady-state pH_i values of C2PLKO.1 and C2NHE2KD cells measured during perfusion with HCO_3^-/CO_2 buffer followed by calibration with pH6.5 and pH7.0 solution gassed with CO_2. Under both condition the steady-state pH_i of C2NHE2KD cells was significantly lower compared to that of C2PLKO.1 cells (n=3–4, mean ± SEM, unpaired student t-test, **p< 0.01).